Journal of Electrochemistry

Volume 28 | Issue 8

2022-08-28

Optimized Electrochemical Performance of Si@C Prepared by Hydrothermal Reaction and Glucose Carbon Source

Si Chen

Song-Sheng Zheng
College of Energy, Xiamen University, Xiamen 361102, P. R. China;, songsheng@xmu.edu.cn

Lei-Ming Zheng

Ye-Han Zhang

Zhao-Lin Wang

Recommended Citation
Si Chen, Song-Sheng Zheng, Lei-Ming Zheng, Ye-Han Zhang, Zhao-Lin Wang. Optimized Electrochemical Performance of Si@C Prepared by Hydrothermal Reaction and Glucose Carbon Source[J]. *Journal of Electrochemistry*, 2022 , 28(8): 2112221.
DOI: 10.13208/j.electrochem.211222
Available at: https://jelectrochem.xmu.edu.cn/journal/vol28/iss8/3

电 化 学
J. Electrochem. 2022, 28(8), 2112221 (1 of 11)

[Article] DOI: 10.13208/j.electrochem.211222 Http://electrochem.xmu.edu.cn

Optimized Electrochemical Performance of Si@C Prepared by Hydrothermal Reaction and Glucose Carbon Source

Si Chen, Song-Sheng Zheng*, Lei-Ming Zheng, Ye-Han Zhang, Zhao-Lin Wang
(*College of Energy, Xiamen University, Xiamen 361102, P. R. China*)

Abstract: Silicon (Si) has been considered as the potential material for the next-generation lithium-ion batteries (LIBs) for its high capacity (4200 mAh·g^{-1}, $Li_{22}Si_5$) and suitable working voltage (about 0.25 V vs. Li/Li$^+$). However, the cycling stability and electrochemical performance of Si anode become significant challenges because of low intrinsic conductivity and huge volume variation (about 400%) during cycling processes. In addition, the repeated formation and destruction of surface solid electrolyte interphase (SEI) film will continuously consume the electrolyte and cause damage to LIBs. Carbon (C) materials, such as graphite, carbon spheres and tubes, have been widely applied to ameliorate the conductivity and restrict the volume change of Si anode, which guarantees electrical performance. Especially, a Si@C core-shell structure is preferred to perform a high capacity and relatively good cycle stability. The hydrothermal process has been commonly used to prepare Si@C anodes for LIBs, therefore, it is significant to optimize the preparing conditions to achieve ideal electrochemical performance. In this study, glucose was taken as the carbon source, using the Si waste from the photovoltaic industry as raw materials to prepare Si@C core-shell structure by hydrothermal process. The preparing parameters have been evaluated and optimized, including temperature, reaction time, raw material composition, and mass ratio.

The optimal preparing process was proceeded in the solution with a glucose concentration of 0.5 mol·L^{-1} and a Si/glucose mass ratio of 0.3. Then, it was treated in a hydrothermal reactor at 190 ℃ for 9 h. The obtained Si@C anode candidate (Sample CS190-3) was tested with a coin half-cell. The specific capacity after the first cycle reached 3369.5 mAh·g^{-1}, and the remaining capacity after 500 cycles 1405.0 mAh·g^{-1} in a current density of 655 mAh·g^{-1}. Moreover, for the rate testing, it retained the discharge capacities of 2328.7 mAh·g^{-1}, 2209.8 mAh·g^{-1}, 2007.1 mAh·g^{-1}, 1769.2 mAh·g^{-1}, 1307.7 mAh·g^{-1} and 937.1 mAh·g^{-1} at the charge rates of 655 mA·g^{-1}, 1310 mA·g^{-1}, 2620 mA·g^{-1}, 3930 mA·g^{-1}, 5240 mA·g^{-1}, and 6550 mA·g^{-1}, respectively. And it was recovered to 1683.0 mAh·g^{-1} when the current density was restored to 655 mA·g^{-1}. In addition, the EIS data revealed that the half-circle radius of the sample obtained by using the optimal conditions (Sample CS190-3) in the low-frequency region was greatly reduced, and the Warburg impedance became the smallest. This work can provide an important approach, and make a significant impact in the preparation of Si/C anode material for LIBs.

Key words: hydrothermal reaction; Si@C ball structure; glucose; anode materials

1 Introduction

Lithium-ion batteries (LIBs) have attracted much attention around the world during the past decades[1-3]. Because of their high capacity, LIBs have been widely used in electronic devices, electric vehicles, and other applications[4]. Graphite is the most common anode material for commercial rechargeable LIBs with stable capacity and reversibility. However, graphite has a low capacity (372 mAh·g^{-1}) and cannot meet the increasing demand[5, 6] in the future, so it is imperative to prepare a new anode with a higher capacity. As an ideal anode candidate, silicon (Si) has a high theoretical capacity (4200 mAh·g^{-1}, $Li_{22}Si_5$)[7, 8]. Unfortunately, a severe volume expansion (> 420%)

Cite as: Chen S, Zheng S S, Zheng L M, Zhang Y H, Wang Z L. The optimal hydrothermal reaction conditions of Si@C ball structures with glucose as carbon source and its electrochemical performance. *J. Electrochem.*, 2022, 28(8): 2112221.

Received: 2021-12-22, Revised: 2022-02-28. *Corresponding author, Tel: (86-592)2188053, E-mail: songsheng@xmu.edu.cn

in Si is inevitable during the lithium intercalation, which will cause high internal stress, electrode pulverization, and consequently loss of electrical contact between the active material and current collector[9-11]. What is worse, solid electrolyte interphase (SEI) films will be constantly generated, resulting in rapid capacity decay, low cycling efficiency, and permanent capacity losses of LIBs[12-14].

Tremendous efforts have been made to solve this volume expansion issue. Nanostructures, such as nanoparticles[15], nanowires[16-19], and nanotubes are promising approaches to minimize the negative effect of the volume expanse. However, the nanomaterials preparation usually needs a complex production process and high cost.

Si/C composites, such as core-shell materials[20-22], nanowires[23], nanotubes[24-27], flakes[28], and spheres[29-31], are one of the potential solutions. Processes of electrochemical deposition[32], laser pyrolysis[33], laser irradiation[34, 35], thermal pyrolysis[36], chemical vapor deposition[37], or chemical etching[37, 38] are usually applied for the fabrication of Si/C composites by using nano Si as a source material. The carbon source seems diverse, such as cellulose[39], glucose[20], starch, dopamine[40, 41], etc. However, the above methods cannot avoid the harsh requirements, including equipment, environment, or raw materials, thus resulting in excessively high cost or meager yields. As a comparison, the mild hydrothermal reaction conditions make it competitive for mass production. On the other hand, the submicron Si recovered from the photovoltaic industry has been proven to be available as Si raw materials for Si/C electrodes in our previous studies[20, 25, 31, 42]. In some other works, the Si@C electrode materials were synthesized successfully. However, the carbon shell was all disordered carbon because the spherical structure is very compact, and it is difficult to change the arrangement of carbon atoms. Due to the increase of sp^2 hybrid ratio of the carbon layer being difficult, the thickness and distribution of the carbon layer have a great influence on the electrochemical performance of the Si@C electrode since a thinner and more uniform carbon layer can provide good electron channels[31]. The hydrothermal reaction conditions are an important part of influencing these factors. It is, therefore, significant to optimize the preparing conditions of the hydrothermal process to achieve ideal electrochemical performance.

In this paper, the submicron Si recovered from the kerf waste of the photovoltaic industry was taken as the raw material, and glucose was used as the carbon source. The Si@C electrodes were prepared by hydrothermal process. The parameters, including temperature, reaction time, and raw material composition, were optimized.

2 Experimental

2.1 Materials Synthesis

Firstly, the Si waste block was ball milled for 10 h at the rate of 200 $r \cdot min^{-1}$, and then cleaned by deionized water to obtain pure submicron Si particles. Secondly, the typical hydrothermal process was as follows by taking the sample CS190-3 as an example: 4.5 g glucose was dissolved in 50 mL deionized water, and 1.35 g ball-milled Si powder was added. After ultrasonic stirring for 20 min, the mixture was transferred into a Teflon-sealed autoclave and placed in an oven at a constant temperature for 9 h, and then cooled naturally to room temperature. The solid was separated by suction filtration and washed with deionized water, and then dried in an oven at 80 ℃ for 12 h. Finally, the precursor was further carbonized under N_2 gas flow at 700 ℃ for 1.5 h. The parameters for the other samples are listed in Table 1.

2.2 Materials Characterizations

SEM images of the as-prepared samples were observed on a Zeiss SUPRA 55 (Carl Zeiss, Germany) field-emission scanning electron microscope (FESEM) equipped with energy-dispersive spectroscopy (EDS). The microstructures of Sample CS190-3 were clarified by TEM (FEI Talos F200S). X-ray diffraction (XRD) patterns were recognized on a Rigaku Ul tima IV diffractometer (Rigaku, Japan) using Cu K_α radiation at 40 kV and 30 mA. Raman spectra were acquired on a LabRAM HR Evolution spectrometer (Jobin Yvon, France) with an argon ion radiation laser beam (excitation wavelength: 633 nm) and an

incident power of 1 mW.

2.3 Electrochemical Measurements

The as-prepared samples were mixed with sodium alginate and conductive carbon black in a mass ratio of 8:1:1, dissolved in deionized water, and mixed for more than 10 h to obtain a black viscous slurry. Then the slurry was coated on the copper foil with a thickness of 100 μm. After drying in a vacuum at 70 °C for 12 h, the foil was cut into 12 mm diameter discs for packaging the battery.

In order to test the electrochemical performance of the as-prepared anode samples, CR2025 coin half-cell was assembled in an argon-filled glove box with lithium metal as the counter electrode and Celgard 2500 diaphragm as the separator. The electrolyte was 1.0 mol·L^{-1} $LiPF_6$ in ethylene carbonate (EC), dimethyl carbonate (DMC), and diethyl carbonate (DEC) (1:1:1 in volume) with 10.0% fluoroethylene carbonate (FEC) and 2.0% vinylene carbonate (VC) additives. The battery was aged for 12 h before testing.

The galvanostatic charge/discharge performances were measured on a LAND-CT2001A battery test system (Wuhan Btrbts Technology Co. Ltd., China) at 30 ℃. The cut-off voltage was set as 0.01 V and 1.2 V vs. Li^+/Li. Furthermore, the electrochemical impedance spectroscopic (EIS) measurements were carried out on a CHI660E electrochemical workstation (Shanghai Chenhua instrument co. Ltd., China) under a frequency range from 0.01 Hz to 100 kHz with an amplitude of 5 mV.

3 Results and Discussion

3.1 Structural Analyses

The XRD and Raman spectra of the samples were obtainedat 200 ℃, and the results are shown in Figure 1. As evident in Figure 1(a), the Si peaks were clearly observed, and a broad carbon peak in $2\theta = 19° \sim 22°$ indicated that the carbon in all the samples was not well crystallized[20]. Simultaneously, the characteristic peaks of Si in the Raman spectra (Figure 1(b)) were located at 512 cm^{-1} and 925 cm^{-1} with the wide D (1337 cm^{-1}) and G bands (1594 cm^{-1}), as well as the large intensity ratios of I_D/I_G as listed in Table 2, which reflected the characteristics of amorphous carbon (or disorder carbon). There was no apparent difference among all the samples, indicating that the structures of the carbon and Si were similar. The differences in

Table 1 Preparation conditions of series samples

Sample	Glucose weight (g)	Silicon weight (g)	Reaction temperature (℃)	Reaction time (h)
CS170-1	2.25	0.9	170	9
CS170-2	4.5	1.35	170	9
CS180-1	2.25	0.9	180	9
CS180-2	4.5	1.35	180	9
CS190-1	2.25	0.9	190	9
CS190-2	4.5	0.9	190	9
CS190-3	4.5	1.35	190	9
CS190-4	4.5	1.8	190	9
CS190-5	4.5	1.35	190	6
CS190-6	4.5	1.35	190	12
CS200-1	4.5	1.35	200	6
CS200-2	4.5	1.35	200	9
CS200-3	2.25	0.9	200	9

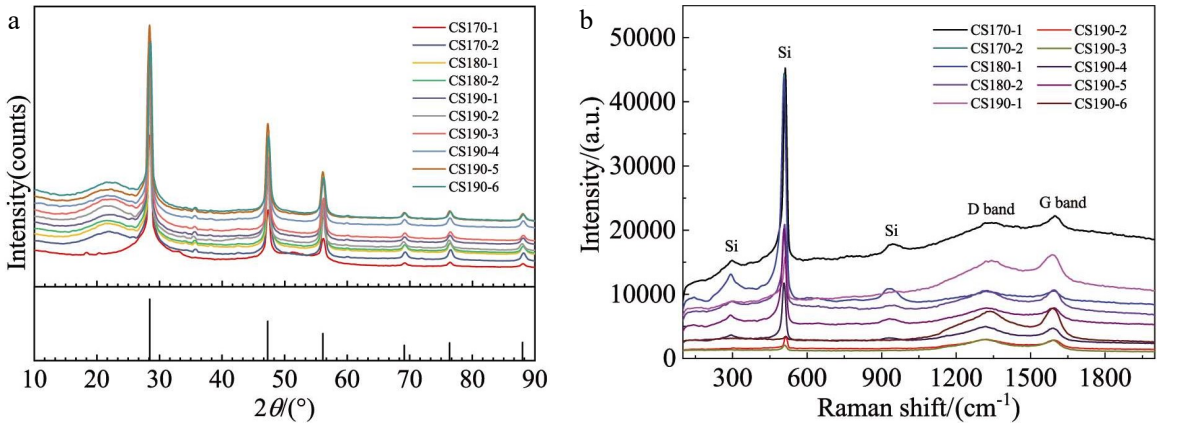

Figure 1 The structure analyses: (a) XRD patterns; (b) Raman spectra (color on line)

Table 2 The I_D/I_G values of the samples determined based on Raman data

Sample	CS170-1	CS170-2	CS180-1	CS180-2	CS190-1	CS190-2	CS190-3	CS190-4	CS190-5	CS190-6
I_D/I_G	0.85	0.85	0.83	0.82	0.84	0.83	0.82	0.84	0.82	0.84

morphology and performance are due to the distribution and thickness of the carbon shell, which will be discussed later.

3.2 The influence of Preparation Conditions on Morphology

The SEM images of the as-prepared samples and EDS data of Sample CS190-3 are shown in Figure 2. Among them, the Si@C ball in Sample CS190-3 exhibited the best spherical morphology, which was uniform, smooth edges, and very few excess flocculent surrounded.

By comparing the samples CS170-2, CS180-2 and CS190-3, it was found that irregular flocculent substances appeared when the hydrothermal reaction temperature was lower than 190 ℃, indicating that the polymerization of glucose in water required the minimum reaction temperature[31, 43]. For the glucose concentration, although Si particles provided the nucleation centers, the furan substances should reach the minimum concentration of nucleation to form solid particles, and the minimum concentration was decreased with the temperature rising. However, the spheres showed a lot of sticking and formed a peanut-like structure when the reaction temperature was 200 ℃ (Sample CS200-2 in Figure 2), indicating that the best reaction temperature was 190 ℃. Moreover, the coating on Si was incomplete when the mass ratio of Si to glucose was 40% (Sample CS190-4 in Figure 2) due to the lack of carbon. On the contrary, when the mass ratio of Si to glucose was 20%, which was too low so that the balls would combine and form a peanut-like structure (Sample CS190-2 in Figure 2).

Furthermore, the morphologies were almost identical when the reaction time was longer than 9 h (Samples CS190-3 and CS190-6 in Figure 2), which indicated that the reaction had been accomplished within 9 h. At the same time, the situation was different when the reaction temperature was 200 ℃. As for the reaction time was 6 h (Sample CS200-1 in Figure 2), there were a lot of small carbon balls with a diameter of about 400 nm (smaller than Si particles) around Si@C balls (diameter more than 3 μm), indicating that under these conditions, carbon spheres were more likely to be formed, rather than a coating on Si. When the glucose concentration was 0.25 mol·L^{-1} at 200 ℃, there were irregular flocculent substances around Si@C balls, indicating that the concentration of glucose was insufficient.

Based on the above results, possible mechanism of forming Si@C core-shell structure is proposed and

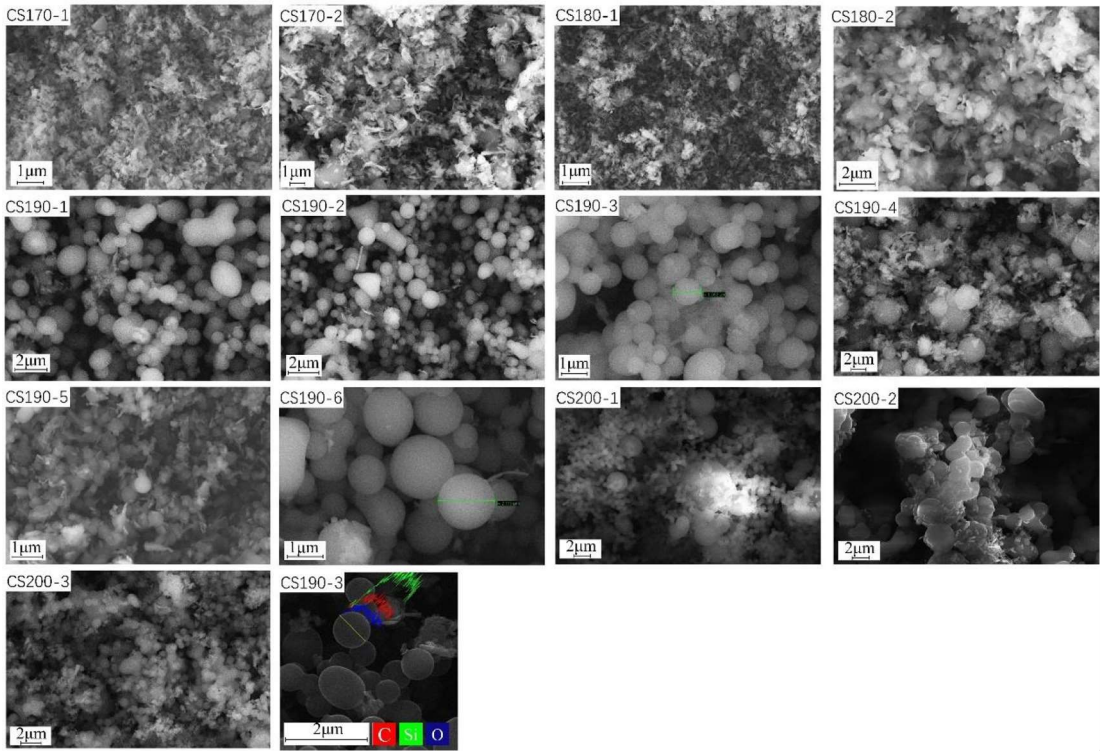

Figure 2 SEM images of the as-prepared samples and EDS result of Sample CS190-3

illustrated in Figure 3. The previous studies suggested that the hydrothermal coating process might include:

(1) The dehydration and condensation reactions of glucose would happen under the catalysis of hydrogen ions provided by water at a high temperature and generate a chain oligomer[14].

(2) The chain oligomer continued to polymerize and form macromolecular solid aromatic compounds following the Lamer model, which was the control step[44].

(3) A coating process of the solid aromatic compound on Si proceeded synchronously by connecting with the functional group on the Si surface[20].

Therefore, the above three reaction steps determine the Si@C core-shell structure and its morphology. Further study on the mechanism is necessary in our future works.

In summary, the optimum process to prepare an ideal Si@C structure with good morphology was by setting the reaction temperature at 190 ℃, the glucose concentration of 0.5 mol·L^{-1}, the mass ratio of Si to glucose as 30%, and the hydrothermal reaction

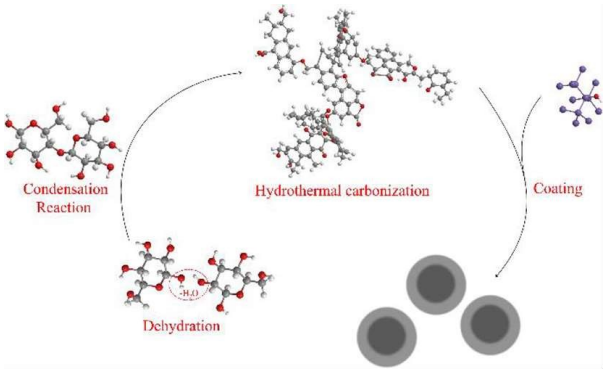

Figure 3 The proposed process of hydrothermal carbonization. (color on line)

time for 9 h.

The TEM images are shown in Figure 4. The Si@C structure was identified in Figure 4 with the thickness of the carbon shell being about 100 nm. Furthermore, a clear boundary between the core and the shell was observed in Figure 4(b), and the lattice fringes with the distances of 0.31 nm and 0.21 nm in Figure 4(c) corresponded to the crystal planes of Si (111) and C (101), respectively. In addition, the lattices

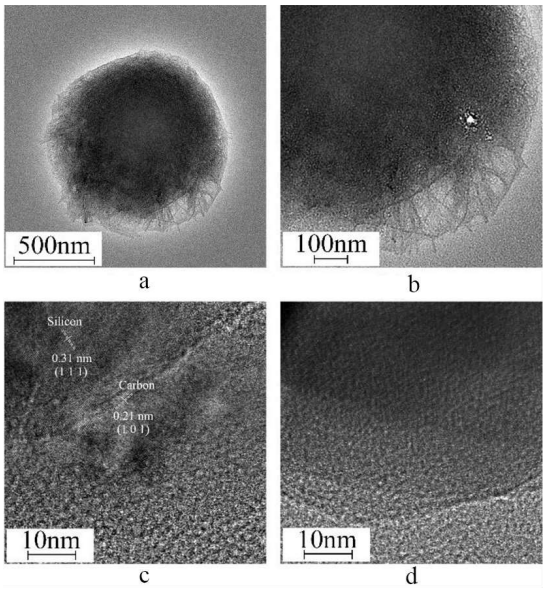

Figure 4 TEM images of Sample CS190-3showing the carbon sphere in Si@C microstructure (a), (b) microstructure; (c), (d) HRTEM images showing the core-sell and boundary in Si@C microstructure

fringes of carbon and Si were partially staggered, indicating that the carbon layer covered the Si tightly without voids. However, the carbon lattices fringes were only observed at the part of the area neighbor to Si (compared Figure 4(c) and Figure 4(d)), thus, the crystallization of the carbon shell was limited.

3.3 The Electrochemical Performance Analyses

The galvanostatic charge/discharge cycle tests and the rate capacity tests were carried out on all the samples with submicron Si electrodes as the reference. As shown in Figure 5(a), the initial specific discharge capacity of Sample CS190-3 was achieved at 3369.5 mAh·g^{-1} with a current density of 655 mA·g^{-1}, which was higher than the electrodes prepared with other samples and the submicron Si electrode. The discharge capacity of Sample CS190-3 electrode still remained 1405.0 mAh·g^{-1} after 500 cycles, which was the highest among all the samples. However, the initial capacities of some other samples were higher than Sample CS190-3, but after 500 cycles, these electrodes all showed severe attenuation. In addition, the coulombic efficiency of the sample CS190-3 at the first cycle was 66.8% (Figure 5(b)) and approached to 100% upon cycling, indicating good reversibility during the charge/discharge process. Therefore, it was determined that a full coating of Si@C could effectively improve the electrochemical performance compared with Si. A carbon layer with moderate thickness and a uniform distribution is more conducive to improving electrochemical performance.

The charge/discharge profiles of Sample CS190-3 at 655 mA·g^{-1} in different cycles are presented in Figure 5(c). It revealed a large capacity loss in the first cycle because of the formation of SEI film. According to the discharge curve, in a voltage range between 0.25 V and 0.01 V, the battery voltage decreased slowly with the increase of the specific capacity, indicating that the battery discharge mainly happened in this voltage range, which corresponds to the process of lithium-ion intercalation in the negative electrode, that is, the process of forming Li_xSi.

The CV curves of the CS190-3 electrode in the first 3 cycles at a sweep speed of 0.2 mV·s^{-1} and a voltage range from 0.01 to 3.0 V are shown in Figure 5(e). There were two reduction peaks at 1.13 V and 0.52 V, which corresponded to the formation of the SEI film, and two oxidation peaks at 0.32 V and 0.52 V, relating to the lithiation and delithiation of Li_xSi alloy, respectively. In addition, the rise of current peaks in the second and third cycles was attributed to electrode activation. However, the curves of the first and second circles had a cross at about 1.0 V, which was caused by the formation of SEI film on the electrode surface during the first discharge.

As shown in Figure 5(c), Sample CS190-3 electrode exhibited the best rate performance. It retained a discharge capacities of 2328.7 mAh·g^{-1}, 2209.8 mAh·g^{-1}, 2007.1 mAh·g^{-1}, 1769.2 mAh·g^{-1}, 1307.7 mAh·g^{-1} and 937.1 mAh·g^{-1} at the current densities of 655 mA·g^{-1}, 1310 mA·g^{-1}, 2620 mA·g^{-1}, 3930 mA·g^{-1}, 5240 mA·g^{-1}, and 6550 mA·g^{-1}, respectively. The recovered discharge capacity of 1683.0 mAh·g^{-1} was obtained when the current density was restored to 655 mA·g^{-1}, which was much better than any other samples.

For the convenience of explanation, the most representative samples (i.e., CS170-2 and CS190-3, representating the products with the worst coating effect and the best preparation process, respectively) were selected for the EIS test. As presented in Figure 5(f), all the EIS curves had a semicircle in the high-frequency region and a slash at the low-frequency region. The R_s value represents the contact resistance (solution resistance), while R_{ct} the resistance of the charge transfer[43, 45]. R_s (contact resistance) is generated by the interface between components inside the battery, and mainly related to battery assembly and electrolyte. R_{ct} (charge transfer resistance) can directly reflect the resistance of the electrode material, and the R_{ct} value of Sample CS190-3 was the lowest, indicating the best conductivity.

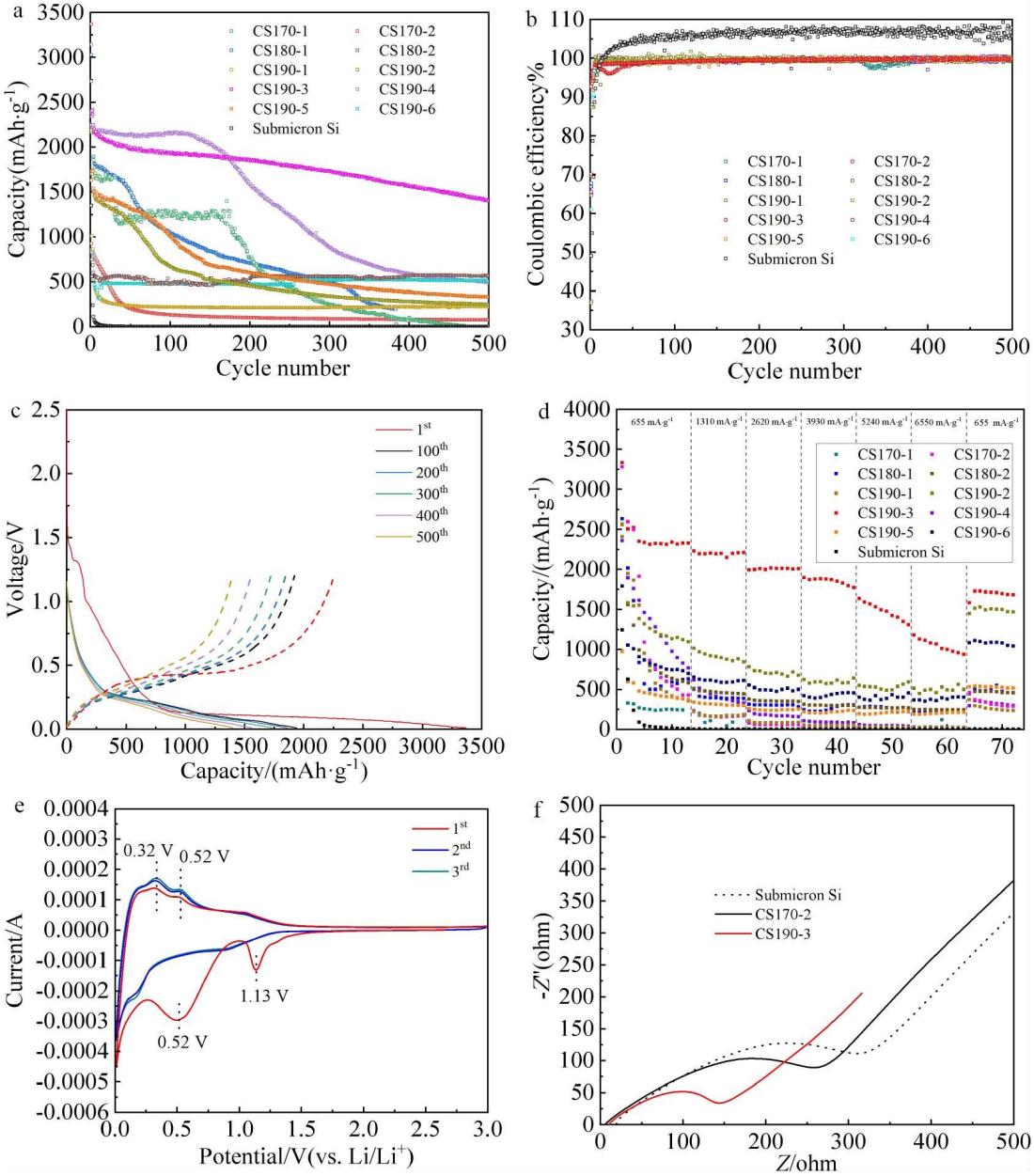

Figure 5 (a) Galvanostatic charge/discharge cycle results of all samples, (b) coulombic efficiency plots of all samples calculated from (a), (c) charge/discharge profiles of galvanostatic charge, (d) rate performance curves of all samples (655 mA·g^{-1}, 1310 mA·g^{-1}, 2620 mA·g^{-1}, 3930 mA·g^{-1}, 5240 mA·g^{-1}, and 6550 mA·g^{-1}), (e) current-voltage curves, (f) Nyquist plots of submicron Si, CS170-2 and CS190-3 electrodes. (color on line)

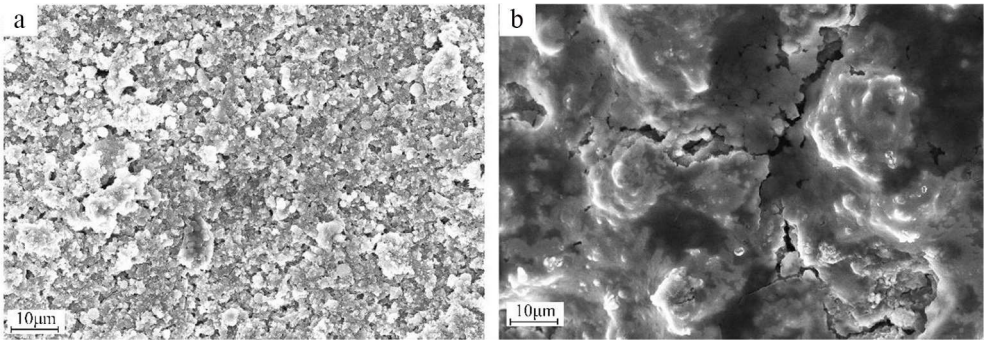

Figure 6 SEM images of Sample CS190-3 electrode before (a) and after (b) cycling.

3.4 SEM Characterizations Before and After Cycling

The electrode surface of Sample CS190-3 (Figure 6(a)) had only minimal gaps. These gaps might be artificially created during the preparation of current collectors and packaging batteries. However, after 500 charge and discharge cycles (Figure 6(b)), the current collectors of Sample CS190-3 showed relatively large cracks, and some intact spheres could be observed within the cracks, indicating that the carbon shell well limited the volume expansion of Si. However, the cracks on the electrode surface became larger, indicating that the Si expansion still caused some damages to the electrode. Moreover, the surface of the electrode showed a morphology covered by dense material, which was caused by the residual electrolyte and the SEI film formed on the electrode surface during the cycling.

4 Conclusions

In this study, glucose was taken as the carbon source to prepare Si@C core-shell structure by hydrothermal process. The preparing parameters including temperature, reaction time, raw material composition, and mass ratio have been evaluated and optimized. As a result, the optimum conditions were determined to be: the reaction temperature of 190 ℃, the glucose concentration of 0.5 mol·L^{-1}, the Si to glucose mass ratio of 30%, and the hydrothermal reaction time of 9 h. The sample CS190-3 was obtained with the optimal conditions. It was found that the CS190-3 electrode exhibited the best electrochemical performance among all the as-prepared anode candidates. It retained a reversible capacity of 1405.0 mAh·g^{-1} after 500 cycles of charge/discharge at a current density of 665 mA·g^{-1}. As for the rate performance, it retained the discharge capacities of 2328.7 mAh·g^{-1}, 2209.8 mAh·g^{-1}, 2007.1 mAh·g^{-1}, 1769.2 mAh·g^{-1}, 1307.7 mAh·g^{-1} and 937.1 mAh·g^{-1} at the current densities of 655 mA·g^{-1}, 1310 mA·g^{-1}, 2620 mA·g^{-1}, 3930 mA·g^{-1}, 5240 mA·g^{-1}, and 6550 mA·g^{-1}, respectively, and could be recovered to the discharge capacity of 1683.0 mAh·g^{-1} when the current density was restored to 655 mA·g^{-1}.

Acknowledgements:

This study was funded by the National Natural Science Foundation of China (21875199), the National "Double First-class"Construction Special Funds Project (0290-X2100502), the College of Energy at the Xiamen University - R & D Center Project of Weifang Sainuo-Kite Broad Spectrum Hydrogen Fuel Cell (XDHT2020024C), the College of Energy at the Xiamen University- R & D Center of Hydrogen Energy of Zibo High Tech Industrial Development Zone (XDHT2020023C), and the Development Project of Energy Research Institute of Hefei Comprehensive National Science Center (XDHT2020305A).

References:

[1] Xu Q, Li J Y, Sun J K, Yin Y X, Wan L J, Guo Y G. Watermelon-inspired Si/C microspheres with hierarchical buffer structures for densely compacted lithium-ion battery anodes[J]. Adv. Energy Mater., 2017, 7(3): 1601481.

[2] Scrosati B, Garche J. Lithium batteries: Status, prospects and future[J]. J. Power Sources, 2010, 195(9): 2419-2430.

[3] Li B, Li S X, Jin Y, Zai J T, Chen M, Nazakat A, Zhan P,

Huang Y, Qian X F. Porous Si@C ball-in-ball hollow spheres for lithium-ion capacitors with improved energy and power densities[J]. J. Mater. Chem. A, 2018, 6(42): 21098-21103.

[4] Kennedy B, Patterson D, Camilleri S. Use of lithium-ion batteries in electric vehicles[J]. J. Power Sources, 2000, 90 (2): 156-162.

[5] Sourice J, Bordes A, Boulineau A, Alper J P, Franger S, Quinsac A, Habert A, Leconte Y, De Vito E, Porcher W, Reynaud C, Herlin-Boime N, Haon C. Core-shell amorphous silicon-carbon nanoparticles for high performance anodes in lithium ion batteries[J]. J. Power Sources, 2016, 328: 527-535.

[6] Liu L H, Lyu J, Li T H, Zhao T K. Well-constructed silicon-based materials as high-performance lithium-ion battery anodes[J]. Nanoscale, 2016, 8(2): 701-722.

[7] Palomino J, Varshney D, Weiner B R, Morell G. Study of the structural changes undergone by hybrid nanostructured Si-CNTs employed as an anode material in a rechargeable lithium-ion battery[J]. J. Phys. Chem. C, 2015, 119(36): 21125-21134.

[8] Luo Z P, Xiao Q Z, Lei G T, Li Z H, Tang C J. Si Nanoparticles/graphene composite membrane for high performance silicon anode in lithium ion batteries[J]. Carbon, 2016, 98: 373-380.

[9] Zhou X S, Yin Y X, Cao A M, Wan L J, Guo Y G. Efficient 3D conducting networks built by graphene sheets and carbon nanoparticles for high-performance silicon anode[J]. ACS Appl. Mater. Interfaces, 2012, 4(5): 2824-2828.

[10] Sun C F, Karki K, Jia Z, Liao H W, Zhang Y, Li T, Qi Y, Cumings J, Rubloff G W, Wang Y H. A beaded-string silicon anode[J]. ACS Nano, 2013, 7(3): 2717-2724.

[11] Ma Z S, Li T T, Huang Y L, Liu J , Zhou Y C, Xue D F. Critical silicon-anode size for averting lithiation-induced mechanical failure of lithium-ion batteries[J]. RSC Adv., 2013, 3(20): 7398-7402.

[12] Lee S W, Mcdowell M T, Choi J W, Cui Y. Anomalous shape changes of silicon nanopillars by electrochemical lithiation[J]. Nano Lett., 2011, 11(7): 3034-3039.

[13] Lux S F, Lucas I T, Pollak E, Passerini S, Winter M, Kostecki R. The mechanism of Hf formation in $LiPF_6$ based organic carbonate electrolyte[J]. Electrochem. Commun., 2012, 14(1): 47-50.

[14] Guo S, Li H X, Bai H M, Tao Z L, Chen J. Ti/Si/Ti sandwich-like thin film as the anode of lithium-ion batteries [J]. J. Power Sources, 2014, 248: 1141-1148.

[15] Choi H S, Lee J G, Lee H Y, Kim S W, Park C R. Effects of surrounding confinements of Si nanoparticles on Si-based anode performance for lithium ion batteries[J]. Electrochim. Acta, 2010, 56(2): 790-796.

[16] Kim H, Cho J. Superior lithium electroactive mesoporous Si@carbon coreshell nanowires for lithium battery anode material[J]. Nano Lett., 2008, 8(11): 3688-3691.

[17] Jeong S, Lee J P, Ko M, Kim G, Park S, Cho J. Etched graphite with internally grown Si nanowires from pores as an anode for high density Li-ion batteries[J]. Nano Lett., 2013, 13(7): 3403-3407.

[18] Liu R P, Shen C, Dong Y, Qin J L, Wang Q, Iocozzia J, Zhao S Q, Yuan K J, Han C P, Li B H, Lin Z Q. Sandwich-like CNTs/Si/C nanotubes as high performance anode materials for lithium-ion batteries[J]. J. Mater. Chem. A, 2018, 6(30): 14797-14804.

[19] Song T, Jeon Y, Paik U. Si nanotubes array sheathed with sin/sioxny layer as an anode material for lithium ion batteries[J]. J. Electroceram., 2014, 32(1): 66-71.

[20] Fan Z Q, Zheng S S, He S, Ye Y Y, Liang J H, Shi A D, Wang Z L, Zheng Z F. Preparation of micron Si@C anodes for lithium ion battery by recycling the lamellar submicron silicon in the kerf slurry waste from photovoltaic industry[J]. Diam. Relat. Mat., 2020, 107: 107898.

[21] Mishra K, Zheng J M, Patel R, Estevez L, Jia H P, Luo L L, El-Khoury P Z, Li X L, Zhou X D, Zhang J G. High performance porous Si@C anodes synthesized by low temperature aluminothermic reaction[J]. Electrochim. Acta, 2018, 269: 509-516.

[22] Yang J P, Wang Y X, Chou S L, Zhang R Y, Xu Y F, Fan J W, Zhang W X, Liu H K, Zhao D Y, Dou S X. Yolk-shell silicon-mesoporous carbon anode with compact solid electrolyte interphase film for superior lithium-ion batteries[J]. Nano Energy, 2015, 18: 133-142.

[23] Bae J. Fabrication of carbon microcapsules containing silicon nanoparticles-carbon nanotubes nanocomposite for anode in lithium ion battery[J]. J. Solid State Chem., 2011, 184(7): 1749-1755.

[24] Xu Q, Li J Y, Yin Y X, Kong Y M, Guo Y G, Wan L J. Nano/micro structured Si/C anodes with high initial coulombic efficiency in Li ion batteries[J]. Chem.-Asian J., 2016, 11(8): 1205-1209.

[25] Liang J, Fan Z, Chen S, Zheng S, Wang Z. A novel three-dimensional cross-linked net structure of submicron Si as high-performance anode for libs[J]. J. Alloy. Compd., 2021, 860: 158433.

[26] Kim J Y, Nguyen D T, Kang J S, Song S W. Facile synthesis and stable cycling ability of hollow submicron silicon oxide-carbon composite anode material for Li-ion battery[J]. J. Alloy. Compd., 2015, 633: 92-96.

[27] Li B, Xiao Z J, Zai J T, Chen M, Wang H H, Liu X J, Li G, Qian X F. A candidate strategy to achieve high initial coulombic efficiency and long cycle life of Si anode materials: Exterior carbon coating on porous Si microparticles[J]. Mater. Today Energy, 2017, 5: 299-304.

[28] Dou X Y, Chen M, Zai J T, De Z, Dong B X, Liu X J, Ali N, Tsega T T, Qi R R, Qian X F. Carbon coated porous silicon flakes with high initial coulombic efficiency and long-term cycling stability for lithium ion batteries [J]. Sustain. Energ. Fuels, 2019, 3(9): 2361-2365.

[29] Wu Z Z, Ji S P, Liu T C, Duan Y D, Xiao S, Lin Y, Xu K, Pan F. Aligned Li^+ tunnels in core-shell $Li(Ni_xMn_yCo_z)O_2$@$LiFePO_4$ enhances its high voltage cycling stability as Li-ion battery cathode[J]. Nano Lett., 2016, 16(10): 6357-6363.

[30] Feng K, Li M, Zhang Y N, Liu W W, Kashkooli A G, Xiao X C, Chen Z W. Micron-sized secondary Si/C composite with *in situ* crosslinked polymeric binder for high-energy-density lithium-ion battery anode[J]. Electrochim. Acta, 2019, 309: 157-165.

[31] Fan Z Q, Wang Y T, Zheng S S, Xu K, Wu J Y, Chen S, Liang J H, Shi A D, Wang Z L. A submicron Si@C core-shell intertwined with carbon nanowires and graphene nanosheet as a high-performance anode material for lithium ion battery[J]. Energy Storage Mater., 2021, 39: 1-10.

[32] Chen X L, Gerasopoulos K, Guo J C, Brown A, Wang C S, Ghodssi R, Culver J N. A patterned 3D silicon anode fabricated by electrodeposition on a virus-structured current collector[J]. Adv. Funct. Mater., 2010, 21(2): 380-387.

[33] Sourice J, Quinsac A, Leconte Y, Sublemontier O, Porcher W, Haon C, Bordes A, De Vito E, Boulineau A, Larbi S J S, Herlin-Boime N, Reynaud C. One-step synthesis of Si@C nanoparticles by laser pyrolysis: High-capacity anode material for lithium-ion batteries[J]. ACS Appl. Mater. Interfaces, 2015, 7(12): 6637-6644.

[34] Momoki K, Manabe T, Li L, Yan J W. Silicon nanoparticle generation and deposition on glass from waste silicon powder by nanosecond pulsed laser irradiation[J]. Mater. Sci. Semicond. Process, 2020, 111: 104998.

[35] Momoki K, Yan J W. Nanoparticle generation from various types of silicon materials by nanosecond-pulsed laser irradiation[J]. Appl. Phys. Express, 2020, 13(2): 026505.

[36] Li X L, Meduri P, Chen X L, Qi W, Engelhard M H, Xu W, Ding F, Xiao J, Wang W, Wang C M, Zhang J G, Liu J. Hollow core-shell structured porous Si-C nanocomposites for Li-ion battery anodes[J]. J. Mater. Chem., 2012, 22 (22): 11014-11017.

[37] Cui L F, Yang Y, Hsu C M, Cui Y. Carbon-silicon core-shell nanowires as high capacity electrode for lithium ion batteries[J]. Nano Lett., 2009, 9(9): 3370-3374.

[38] Han H, Huang Z P, Lee W. Metal-assisted chemical etching of silicon and nanotechnology applications[J]. Nano Today, 2014, 9(3): 271-304.

[39] Shen D Z, Huang C F, Gan L H, Liu J, Gong Z L, Long M N. Rational design of Si@SiO_2/C composites using sustainable cellulose as a carbon resource for anodes in lithium-ion batteries[J]. ACS Appl. Mater. Interfaces, 2018, 10(9): 7946-7954.

[40] Wu J, Tu W M, Zhang Y, Guo B L, Li S S, Zhang Y, Wang Y D, Pan M. Poly-dopamine coated graphite oxide/silicon composite as anode of lithium ion batteries [J]. Powder Technol., 2017, 311: 200-205.

[41] Yu H J, Li X T, Fang H, Chen Q Y, Jiang F, Shao G. Gold/silicon nanocomposites: synthesis, characterization, and application in detection of dopamine[J]. Mater. Sci., 2011, 22(6): 690-693.

[42] Liang J H, Chen S, Fan Z Q, Zheng S S, Wang Z L. N-doped C/Si@damo composite material using PVP as the carbon source for lithium-ion batteries anode[J]. Ionics, 2021, 27(10): 4185-4196.

[43] Bhagavannarayana G, Sharma S N, Sharma R K, Lakshmikumar S T. A comparison of the properties of porous silicon formed on polished and textured (100) Si: High resolution XRD and PL studies[J]. Mater. Chem. Phys., 2006, 97(2-3): 442-447.

[44] Sevilla M, Fuertes A B. Chemical and structural properties of carbonaceous products obtained by hydrothermal carbonization of saccharides[J]. Chem.-Eur. J., 2009, 15(16): 4195-4203.

[45] Huang Y, Pemberton J E. Synthesis of uniform, spherical sub-100nm silica particles using a conceptual modification of the classic lamer model[J]. Colloid Surf. A-Physicochem. Eng. Asp., 2010, 360(1-3): 175-183.

水热法制备锂电池 Si@C 负极材料的工艺优化研究

陈 思,郑淞生*,郑雷铭,张叶涵,王兆林
(厦门大学能源学院,福建 厦门 361102)

摘要: 水热法是广泛应用于锂离子电池 Si@C 电极材料的一种制备方法, 其反应条件是影响产物最终形貌和性能的重要因素, 采取最佳的反应工艺可以大大提升材料的电化学性能。本研究中, 使用葡萄糖作为碳源, 光伏切割废料硅为硅源, 探究了水热法制备核壳结构 Si@C 电极材料的最优工艺, 分别研究了温度、原料浓度、反应时间和原料比例对产物的形貌、性能的影响以及相互之间的关系, 并得到最佳反应条件。在该条件下(葡萄糖浓度为 0.5 mol·L^{-1}, 硅与葡萄糖重量比为 0.3:1, 反应温度190 ℃, 反应时间 9 h), 得到了包覆完整、粒径适中的 Si@C 电极材料(CS190-3), 对以该样品为负极的扣式半电池进行电化学测试, 在 655 mA·g^{-1} 的电流密度下, 其首圈放电比容量为 3369.5 mAh·g^{-1}, 经过 500 次循环剩余容量为 1405.0 mAh·g^{-1}。倍率测试中, 在 6550 mA·g^{-1} 的电流密度下,其剩余容量为 937.1 mAh·g^{-1},当电流密度恢复至 655 mA·g^{-1} 时,电池放电比容量仍可恢复至 1683.0 mAh·g^{-1}。

关键词: 水热反应;核壳结构 Si@C 材料;葡萄糖;锂离子电池负极材料